Journal of the European Ceramic Society **19** (1999) 2337–2348

PII: S0955-2219(99)00099-0
0955-2219/99/$ - see front matter

Kinetics of Phase Transformations in SiAlON Ceramics: II. Reaction Paths

Anatoly Rosenflanz† and I.-Wei Chen*

Department of Materials Science and Engineering, University of Pennsylvania, Philadelphia, PA 19104-6272, USA

Abstract

Kinetics of various α/β-Si_3N_4→α′/β′-SiAlON transformations were investigated for SiAlON ceramics with additions of rare-earth cations. It was determined that α-Si_3N_4 starting powders lead to faster Si_3N_4→α′/β′-SiAlON transformations than β-Si_3N_4 powders. In reactions with a two-phase α′/β′-SiAlON product, the formation of a SiAlON that is structurally similar to the majority starting powders is initially favored, and such SiAlON has a solute composition leaner than the final equilibrium composition. These results suggest that the transformation kinetics is largely governed by the heterogeneous nucleation that is strongly sensitive to the driving force, dictated by the majority phase of the starting powders, and that coherent nucleation is often favored when abundent isostructural nucleation sites are available. © *1999 Elsevier Science Ltd. All rights reserved.*

Keywords: kinetics, nucleation, phase transformations, sialon, Si_3N_4.

1 Introduction

Silicon nitride and its solid solutions are important structural ceramics that exhibit excellent strength, toughness, hardness and processability. There are two polymorphs of silicon nitride, α-Si_3N_4 and β-Si_3N_4, which differ in structure by stacking sequences. They each form solid solutions commonly referred to as α'-SiAlON and β'-SiAlON. Since silicon nitride and SiAlON ceramics are usually prepared from α-Si_3N_4 or β-Si_3N_4 powders, but the final phase can be either $\alpha'-$ or β'-SiAlON, phase transformations are commonly encountered and are an integral part of processing. It is therefore necessary to obtain an understanding of these transformations in order to provide a knowledge base for sintering and hot pressing these ceramics.

The phase transformations in these ceramics generally occur via a solution-reprecipitation mechanism in the presence of a liquid.[1] Solid state transformation is regarded as too sluggish for silicon nitride system. In this connection, diffusion (or the viscosity of the liquid) and the solubility of various constituent species in the liquid are important considerations for the kinetics of transformations. These considerations are all composition and temperature dependent and are rather complicated. We, however, have found it possible to correlate the transformation kinetics with the overall energetics. In the preceding paper (hereafter referred to as paper I) we have monitored the kinetics of phase transformation as a function of overall composition and temperature and showed that the above correlation holds. In the present paper we will further monitor the transformation kinetics as a function of reaction paths to try to establish a similar correlation. Although the above approach is incomplete in that it overlooks the processes that take place in the liquid, it can nevertheless be justified in terms of nucleation and growth kinetics as we will demonstrate below. It will be shown that the overriding consideration in many such reactions is the net driving force from the initial to the final states.

Using nominal α-Si_3N_4 or β-Si_3N_4 starting powders, four possibilities of forming SiAlON solid solutions present themselves:

α-Si_3N_4→α'-SiAlON (1)
α-Si_3N_4→β'-SiAlON (2)
β-Si_3N_4→β'-SiAlON (3)
β-Si_3N_4 →α'-SiAlON (4)

The above transformations should be understood as including other reactants and products to account for conservation of mass. For example, in

*To whom correspondence should be addressed. Fax: +1-215-573-2128; e-mail: iweichen@seas.upenn.edu
†Currently with 3M Corp, St. Paul, MN, USA

transformations (2) and (3), Al and O must be incorporated through the addition of Al_2O_3, AlN, and residual SiO_2, while the balance of the additives and the reactants must themselves regroup in the form of other products such as a glassy phase or an AlN polytypoid. The energetics of these transformations can be classified in terms of the energy difference between the initial, intermediate and final states using the following considerations.

First, since α-Si_3N_4 is unstable with respect to β-Si_3N_4,[2], a larger driving force should be present for transformations involving α-Si_3N_4 powder, i.e for transformations (1) and (2), compared to transformations (3) and (4). We will refer to this driving force as ΔG, which accounts for the end-state thermodynamics with reference to the initial state and is dependent on the composition, the majority phase of the starting Si_3N_4 powders, and temperature only. This ΔG is independent of the intermediate steps of dissolution and reprecipitation and the intermediate phase of supersaturated liquid, since, after sufficient dissolution, starting powder and the supersaturated liquid may reasonably be regarded as being in equilibrium with each other. Under such circumstances, the driving force of reprecipitation is precisely the free energy difference between the starting Si_3N_4 powder and the final SiAlON phase.

Second, transformations that occur by solution-reprecipitation require a new phase nucleated from the oxide melt either homogeneously or heterogeneously. Transformations between phases of the same structure, i.e. $\alpha \rightarrow \alpha'$ (1) and $\beta \rightarrow \beta'$ (3), will most likely take advantage of heterogeneous nucleation on sites of existing isostructural particles [α-Si_3N_4 for reaction (1) and β-Si_3N_4 for reaction (3)].[3,4] Thus, in theory, reactions (1) and (3) should have an advantage compared with those involving different structures, i.e. $\alpha \rightarrow \beta'$ (2) and $\beta \rightarrow \alpha'$ (4). In reality, however, both nominal α-Si_3N_4 and nominal β-Si_3N_4 powders contain a small amount of admixed phases (5 wt% of β-Si_3N_4 in our α-Si_3N_4 powders and 7 wt% of α-Si_3N_4 in our β-Si_3N_4 powders), which could provide the sites for heterogeneous nucleation on isostructural particles even when the overall transformation involves mostly phases with dissimilar structures. Therefore, we expect that the path of nucleation is roughly identical in reactions (1) and (4), and (2) and (3). Of course, the driving force ΔG has a large influence on the magnitude of nucleation barrier, ΔE_a: the larger the ΔG, the smaller the ΔE_a for the same nucleation path. As mentioned above, the driving force is dependent on the majority phase of the starting Si_3N_4 powders. Therefore, transformations (1) and (2) could enjoy a smaller activation energy for nucleation compared to transformations (3) and (4). The above considerations involving energetics of reactions 1–4 are schematically illustrated in Fig. 1. It suggests that, due to a larger ΔG, reaction (1) and (2) have an advantage over reactions (3) and (4) both in a smaller nucleation barrier and in a larger growth force. A major difference, however, may also exists between reactions (1) and (2), in that there are many more sites available for nucleation in reaction (1) than in reaction (2). [Likewise, there are more nucleation sites in reaction (3) than in reaction (4).] These favorable nucleation statistics are expected to facilitate transformation kinetics in reactions (1) and (3).

In the following, we perform a series of experiments to assess the overall kinetics of reactions (1)–(4). The

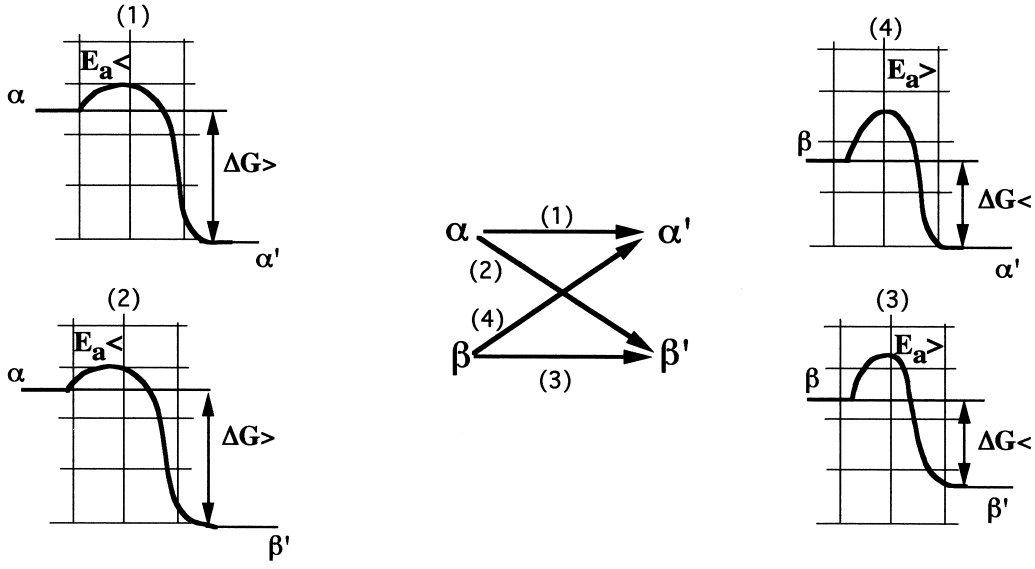

Fig. 1. Schematic energy diagrams for typical reactions in SiAlON systems. ΔG is assigned according to the starting powder. ΔE_a is assigned according to ΔG and assuming heterogeneous sites, isostructural with the product phase, are available. Grid is in arbitrary units.

results indicate that the kinetics follow the order of (1) > (2) > (3) > (4), suggesting that the driving force is the primary consideration and the site statistics is of secondary importance. These results will be rationalized in terms of nucleation theory. In practice, reactions (1) and (4), and reactions (2) and (3), can be compared directly by choosing different starting powders (α and β-Si_3N_4). Here, we will take the precaution of comparing powders of comparable sizes, but we will also be cognizant of the consequences of different particle sizes when they arise. A direct comparison of transformations (1) and (2), or (3) and (4), on the other hand, must be made with reaction products that contain a two-phase mixture; that is, transformations (1) and (2) cannot be separately conducted using the same composition. This is because in compositions that have only a single phase reaction product, the equilibrium phase is either α'-SiAlON or β'-SiAlON, but not both. Likewise, kinetics of transformations (3) and (4) can be compared using compositions that yield two equilibrium phases in the final state.

2 Experimental

2.1 Composition

The overall compositions studied here lie on the so-called α'-SiAlON plane, which is defined as $R_{m/3}Si_{12-(m+n)}Al_{m+n}O_nN_{16-n}$ with m and n as variables and R a rare-earth ion. The experimentally accessible range of these compositions is bounded between Si_3N_4–4/3(AlN:Al_2O_3) line and Si_3N_4—$M_{3/z}$N:3AlN line, with Si_3N_4 as the apex. The actual range of α'-SiAlON existence (i.e. the single phase α'-SiAlON region which is itself represented as $R_{m/3}Si_{12-(m+n)}Al_{m+n}O_nN_{16-n}$) is schematically shown in Fig. 2 for rare-earth cations and is restricted to a fan-shaped area bordered by the Si_3N_4–RN:3AlN line.

The line of Si_3N_4–4/3(AlN:Al_2O_3) coincides with the single phase β'-SiAlON region, which is represented by $Si_{6-x}Al_xO_xN_{8-x}$ with $0 \leq \times \leq 4{\cdot}2$. In this study, we have examined compositions in both single phase and two-phase SiAlON ceramics, with R = Nd, Yb, and Y. These compositions are believed to be representative of a broad range of SiAlON compositions. As in paper I, we will refer to compositions of $R_{m/3}Si_{12-(m+n)}Al_{m+n}O_nN_{16-n}$ as $R-10m10n$. For example, Yb-1020 means that R = Yb, $m = 1{\cdot}0$ and $n = 2{\cdot}0$. In addition, some compositions along the β'-SiAlON line ($m-0$) were also investigated.

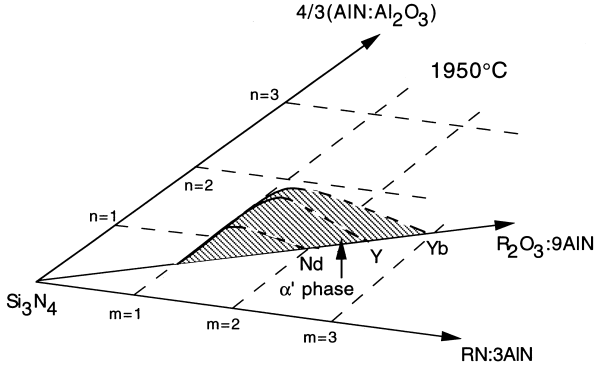

Fig. 2. Portion of the phase diagram on the α'-SiAlON plane at 1950°C, showing that the α'-region is smaller for larger rare-earth cations.

2.2 Experimental procedures

All powder processing, hot-pressing, heat-treatment and characterization procedures employed for this work were identical to those already discussed in paper I (see Section II therein).

3 Results

3.1 Reactions (1) and (2)

We first compare transformations (1) and (2) using Yb-0618, Y-0718 and Nd-0818 compositions prepared with α-Si_3N_4 starting powders. According to the phase diagram in Ref. 5, at 1700°C these compositions should yield a phase mixture of α'-SiAlON and β'-SiAlON. Figure 3 depicts α'/β'-SiAlON phase evolutions as a function of the annealing temperature. It is evident from this figure that at low temperatures the α'-SiAlON formation curves always lie above the β'-SiAlON formation curves, indicating that the kinetics of $\alpha \rightarrow \alpha'$ transformation (1) is faster than that of $\alpha \rightarrow \beta'$ transformation (2). In fact, the initial kinetic advantage of transformation (1) is manifested even when less α'-SiAlON than β'-SiAlON is eventually obtained, as in the case of Fig. 3(c). Note transformations (1) and (2) have the same driving force (α' in equilibrium with β'), but the number of available sites for nucleation is probably greater in (1) than in (2). Thus, the different kinetics seem to reflect the different nucleation statistics.

3.2 Reactions (2) and (3)

We next compare transformations (2) and (3) using Yb-0625, Y-0625 and Nd-0625 compositions but with different starting Si_3N_4 powders. At equilibrium at 1800°C, this composition should yield nearly single phase α'-SiAlON, except in the case of Yb, where up to 25 wt% of α'-SiAlON phase is expected to form. As illustrated in Fig. 4, when the starting powder is α-Si_3N_4 [reaction (2)], β'-SiAlON generally forms faster than when the starting powder is β-Si_3N_4 [reaction (3)]. For instance, if we denote the temperature at which 50 wt% of β'-SiAlON forms as T_{50}, then the T_{50} of reaction (2) — 1580°C for

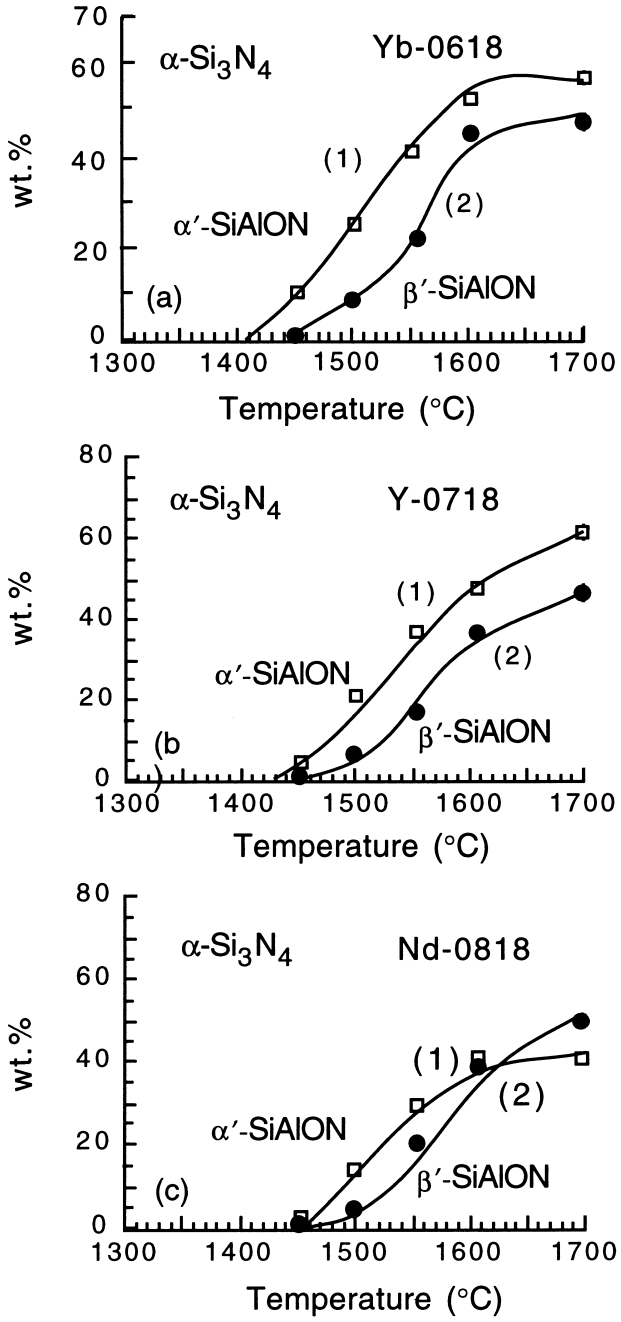

Fig. 3. Phase development from α-Si_3N_4 starting powder in (a) Yb-0618 composition, (b) Y-0718 composition and (c) Nd-0818 composition. At lower temperatures, structurally related phases form first in all cases.

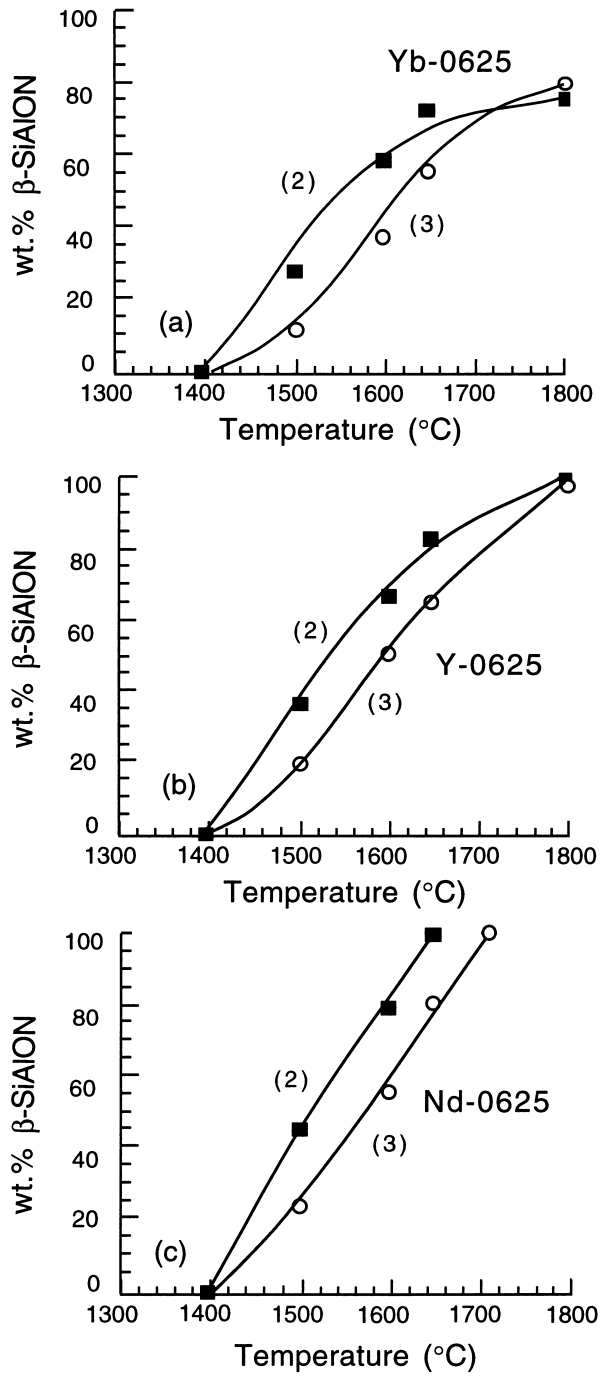

Fig. 4. Kinetics of α/β-$Si_3N_4 \rightarrow \beta'$-SiAlON transformations in (a) Yb-0625 composition, (b) Y-0625 composition and (c) Nd-0625 composition. α-powder [reaction (2)] converts faster than β-powder [reaction (3)].

Yb-0625, 1525°C for Y-0625 and 1495°C for Nd-0625—is consistently lower than the T_{50} of reaction (3) — 1620°C for Yb-0625, 1585°C for Y-0625 and 1560°C for Nd-0625 compositions. Thus, the kinetics of $\alpha \rightarrow \beta'$ transformation (2) is faster than that of $\beta \rightarrow \beta'$ transformation (3).

It is noted that T_{50} in either reaction (2) or (3) is consistently lower for compositions with lighter rare-earth cations. This is probably a result of lower viscosity of the glassy phase which contains lighter rare-earth cations (see Appendix to paper I). Unlike α'-SiAlON, which requires rare-earth cations as stabilizers, β'-SiAlON can form without using any rare-earth oxides. This provides us the opportunity to compare reactions (2) and (3) without any complication due to viscosity. The composition we chose for this study is $Si_{4.5}Al_{1.5}O_{1.5}N_{6.5}$. It is seen from Fig. 5 that the kinetics of $\alpha \rightarrow \beta'$ transformation is again faster than that of $\beta \rightarrow \beta'$ transformation [$T_{50} = 1550$°C for (2) and 1585°C for (3)].

Transformation (2) is expected to have a larger ΔG, a smaller ΔE_a, but fewer sites for isostructural nucleation than transformation (3). The observation

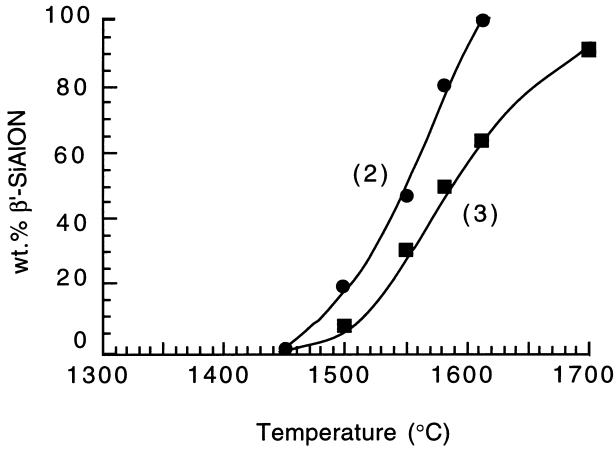

Fig. 5. Kinetics of $\alpha/\beta \rightarrow \beta'$-SiAlON transformation in $Si_{4.5}Al_{1.5}O_{1.5}N_{6.5}$ composition. Higher ΔG of reaction (2) affects kinetics more than higher nucleation statistics of reaction (3).

that transformation (2) proceeds faster than transformation (3) suggests that the driving force advantage (which also influences ΔE_a) outweighs the nucleation statistics disadvantage in these reactions.

3.3 Reactions (3) and (4)

Reactions (3) and (4) can be compared using compositions Yb-0618, Y-0718 and Nd-0818. These are the same compositions used for comparing reactions (1) and (2), but they are now prepared from β-Si_3N_4 starting powder. With β-Si_3N_4 powders, we found it difficult to form α'-SiAlON at lower temperatures. Therefore, the final annealing temperature was raised to 1800°C for Yb-0618 and Y-0718 and to 1900°C for Nd-0818. (Phase diagrams[5,6] indicate that an α'/β' SiAlON mixture should still be obtained at these temperatures.) Figure 6 demonstrates that β'-SiAlON formation curves always lie above the α'-SiAlON formation curves indicating that the kinetics of $\beta \rightarrow \beta'$ transformation (3) is faster than that of $\beta \rightarrow \alpha'$ transformation (4). Indeed, the difference in the transformation kinetics, as indicated by T_{50} of the two curves is relatively large in all the cases. Since the ΔG and ΔE_a are presumably the same for the two reactions (α' and β' are in equilibrium with each other), but there are more sites for isostructural nucleation in reaction (3), the faster kinetics of reaction (3) seems to reflect the advantage in nucleation site statistics.

3.4 Reactions (1) and (4)

Transformations (1) and (4) were compared directly, using Yb-1212, Y-1212 and Nd-1212 compositions but with different starting Si_3N_4 powders. At sufficiently high temperature (1950°C), all these compositions should yield single phase α'-SiAlON independent of the type of reaction. We see from Fig. 7(a)–(c) that the kinetics of $\alpha \rightarrow \alpha'$ transformation (1), given by $T_{50} = 1475$°C

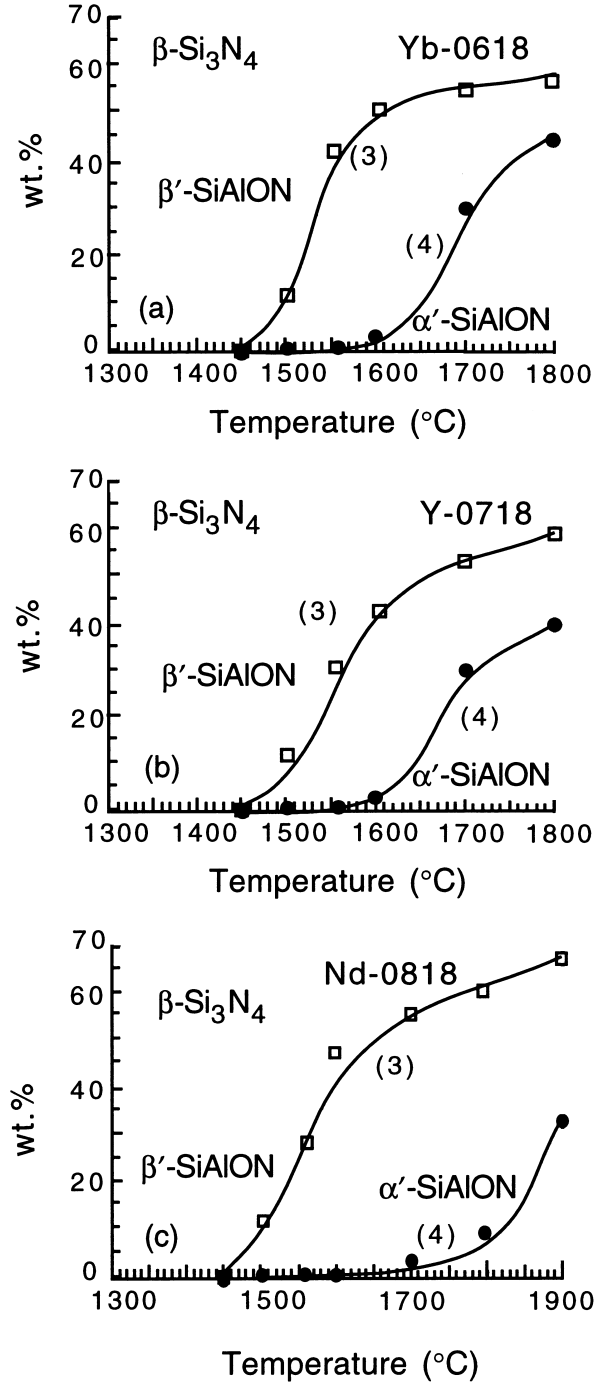

Fig. 6. Phase development from β-Si_3N_4 starting powder in (a) Yb-0618 composition, (b) Y-0718 composition and (c) Nd-0818 composition. At lower temperatures, structurally related phases form first in all cases.

for Yb-1212, 1500°C for Y-1212 and 1625°C for Nd-1212 composition, is faster than that of $\beta \rightarrow \alpha'$ transformation (4), given by $T_{50} = 1525$°C for Yb-1212, 1575°C for Y-1212, and above 1700°C for Nd-1212. Thus, transformation (1), proceeds faster than transformation (4).

Contrary to results in Fig. 4, we find in Fig. 7 the Yb composition reacts at a lower temperature than the Nd composition, with the Y-composition falling between them. This cannot be attributed to the effect of viscosity, since Nd silicates are expected to be less viscous. The observation can nevertheless be

explained by the different stability of α'-SiAlON, which favors smaller rare-earth cations in the solid solution. As shown previously in paper I, the transformation kinetics of the more stable phase proceeds faster.

In paper I we have also pointed out that the magnitude of ΔG in general will depend on the composition of α'-SiAlON phase. For example, composition Yb-1212, which lies well inside the single phase α'-SiAlON field,[5] is more stable than Yb-1020, with a composition near the boundary of α'-SiAlON. Thus, ΔG in Yb-1020 composition is smaller than the ΔG in Yb-1212 composition for both reactions (1) and (4). This is reflected in Fig. 8, in which we see that both reactions have been delayed compared to Fig. 7(a). Note, however, that T_{50} in reaction (4) has been delayed by 200°C from 1540°C in Fig. 7(a) to 1740°C in Figs. 8, but T_{50} in reaction (1) seems to have hardly changed in Fig. 7 and 8. Thus, a smaller driving force is particularly disadvantageous for transformations that have slower kinetics but is less consequential for transformations that have faster kinetics. As illustrated in Fig. 1, transformation (1) has a higher ΔG and a smaller ΔE_a than transformation (4). It probably also has more available sites for isostructural nucleation than transformation (4). Both advantages suggest faster kinetics for transformation (1) than for (4), in agreement with the above observations.

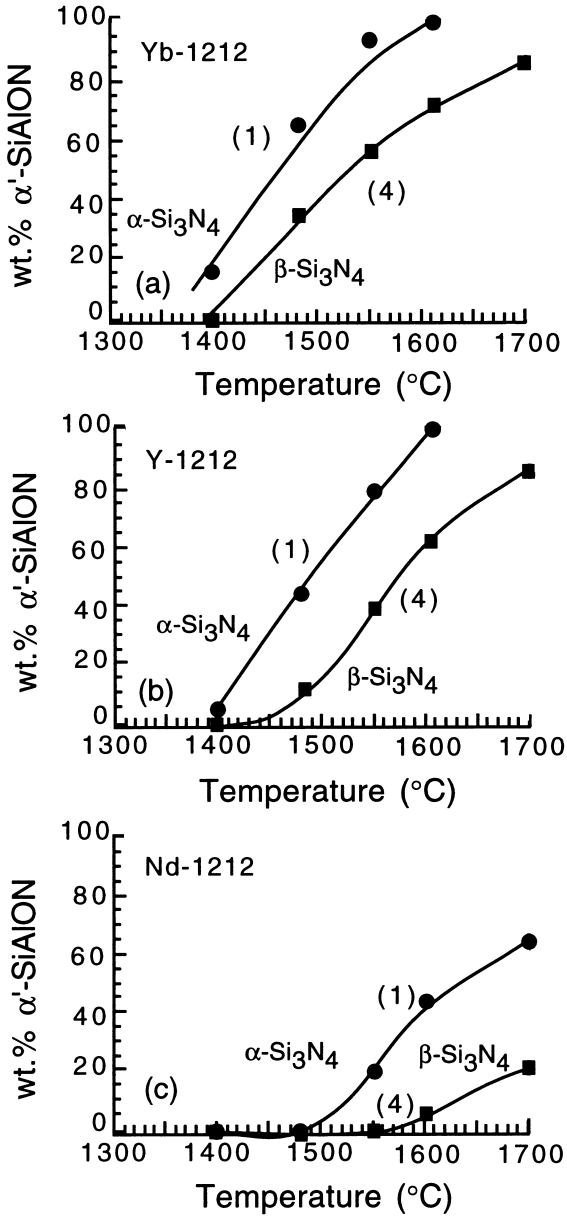

Fig. 7. Kinetics of $\alpha/\beta \rightarrow \alpha'$-SiAlON transformations in (a) Yb-1212 composition, (b) Y-1212 composition and (c) Nd-1212 composition. α-powder converts much faster than β-powder.

3.5 Particle size effect

Particle size is a physical consideration independent of composition. A smaller particle size generally enhances the kinetics of transformation,[7] but it should have only a small effect on the driving force. (We assume the capillarity effect is small.) The particle size effect was analyzed in this work by comparing transformation rates of R-1212 composition, with R = Yb, Er, Y, Dy, Gd, Sm and Nd, prepared with fine α-Si_3N_4 (UBE SN-E10) and coarse α-Si_3N_4 (UBE SN-E-03) powders. (These compositions should yield single phase α'-SiAlON at sufficiently high temperature.) We found that α'-SiAlON forms more slowly when fine α-Si_3N_4 powder is substituted by coarse α-Si_3N_4 powder, probably due to slower dissolution rates of the coarse powder. However, in all cases, the coarse α-Si_3N_4 powders (1.5 μm) still react faster than the fine β-Si_3N_4 powders (0.5 μm) in the formation of α'-SiAlON. These results are summarized in Fig. 9. Thus, even when the average particle size of starting α-Si_3N_4 powder is at least three times that of the β-Si_3N_4 powder, α-Si_3N_4 still transforms to α'-SiAlON faster. The latter observation unequivocally shows that the advantage of reaction (1) over reaction (4) is overwhelming, and the favorable

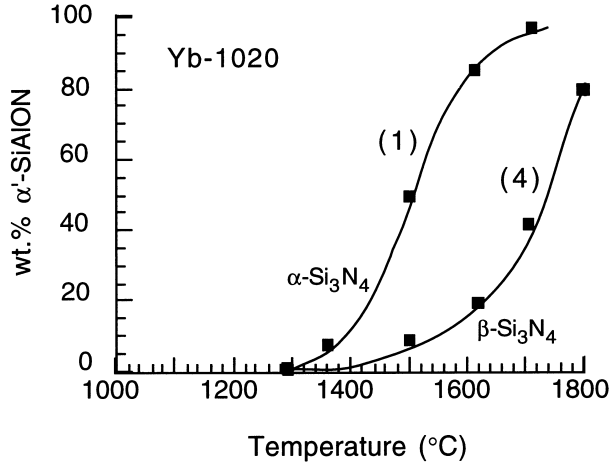

Fig. 8. Kinetics of $\alpha/\beta \rightarrow \alpha'$-SiAlON transformation in Yb-1020 composition prepared from α-powder [reaction (1), $T_{50} = 1500$°C] and β-powder [reaction (4), $T_{50} = 1740$°C].

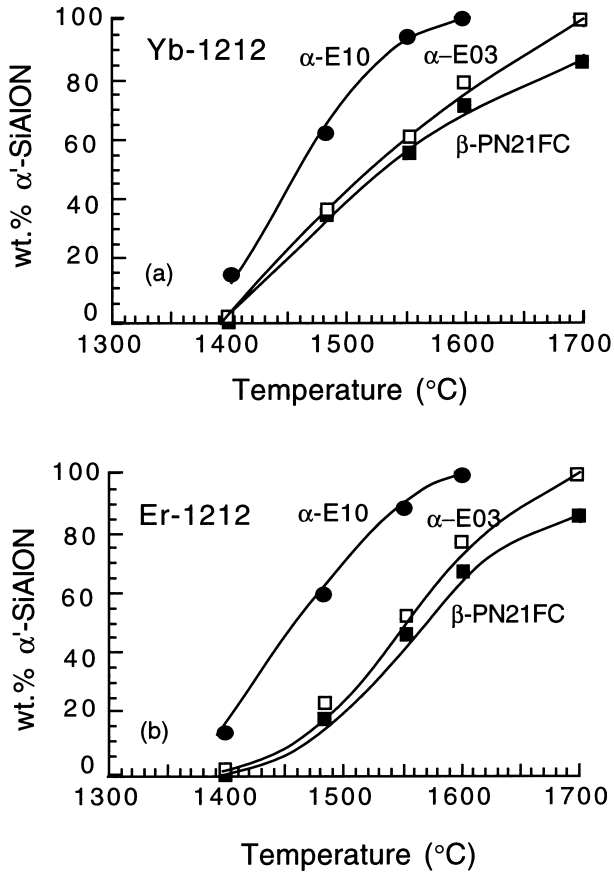

Fig. 9. Kinetics of α'-SiAlON formation with three different starting powders. In all cases, α-powder transforms faster than β-powder. (a) Yb-1212 composition, (b) Er-1212 composition.

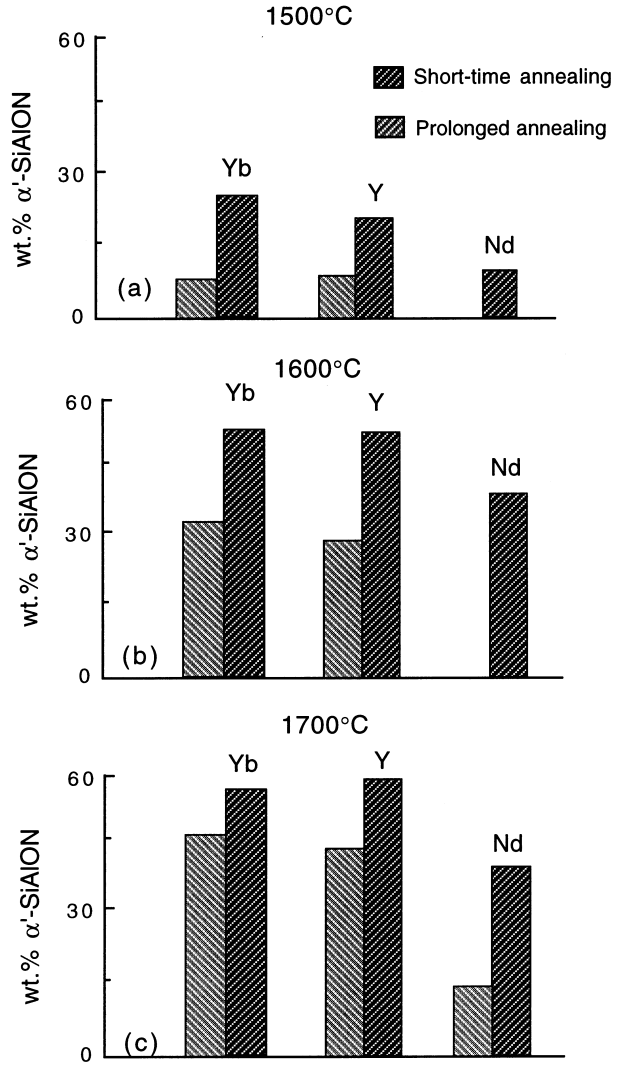

Fig. 10. Amount of α'-SiAlON formed from α-Si_3N_4 powder compared after 45 min and longer annealing time (see text) in Yb-0618, Y-0718 and Nd-0818 materials at (a) 1500°C, (b) 1600°C and (c) 1700°C.

transformation kinetics cannot be easily negated by varying the particle size by up to a factor of 3.

3.6 Transient evolutions

In the course of investigating two-phase reactions (1)–(2) and (3)–(4), we noticed some interesting features in phase assemblages and lattice parameters that may indicate transient evolutions departing from the equilibrium ones as dictated by the phase diagram. These transient evolutions are described below.

One trend we noticed is that the product SiAlON phase that is structurally related to the majority of the starting powders and that forms more rapidly initially forms at an amount exceeding the value expected from phase equilibrium and with a composition leaner in the solutes. This trend is especially pronounced at lower temperatures. In the case of α-starting powder [reactions (1) and (2)] for instance, Fig. 10 shows that the amount of α'-SiAlON precipitating from α-Si_3N_4 during short time annealing was higher than the amount of α'-SiAlON eventually obtained after long-time annealing (240 h at 1500°C, 120 h at 1600°C and 50 h at 1700°C). These initial α'-SiAlON precipitates are leaner in solute content than in the equilibrium phase assemblage, resulting in a broad XRD spectrum that extends to higher 2θ values. Figure 11 shows the XRD of Yb-0618 material prepared from α-Si_3N_4 powder annealed at 1600°C for 45 min and 120 h. As evident from this figure, reflections from (102) and (210) planes of α'-SiAlON formed during the first 45 min are much broader than those of α'-SiAlON formed after 120 h, the latter having a sharp XRD peaking at lower 2θ values. (All solutes in α'-SiAlON tend to dilate the lattice, i.e. the lattice parameters increase with both m (very strongly) and n (weakly).) In contrast, the reflections of structurally unrelated β'-SiAlON does not show any important shift in the XRD pattern.

Similarly, for reactions (3) and (4), we see in Fig. 12 in the Yb-0618 composition that during early transformation the β'-SiAlON phase formed from structurally related β-Si_3N_4 powder has a broader range of compositions than does the equilibrium phase, as illustrated by β'-SiAlON (101) and (210)

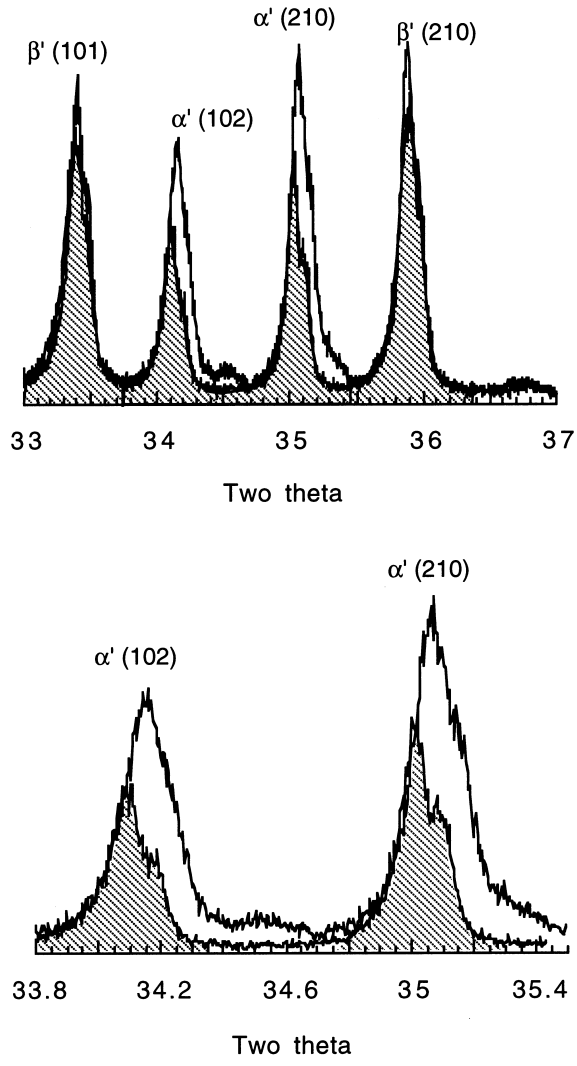

Fig. 11. X-ray diffraction patterns of Yb-0618 material prepared from α-Si_3N_4 powder at 1600°C for 120 h (highlighted) and 45 min. Broader α' reflections in the latter case indicate that transient α'-SiAlON has a range of compositions.

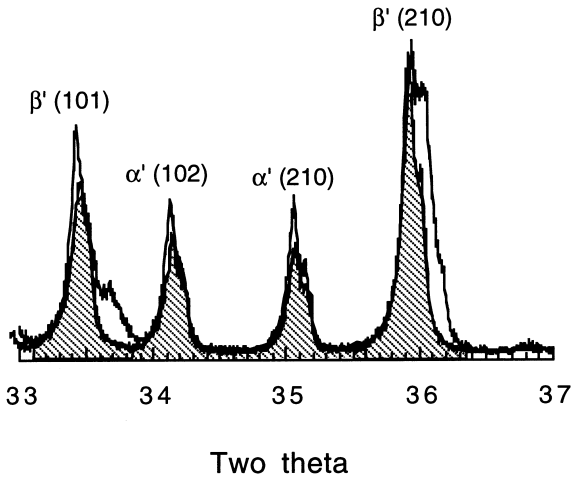

Fig. 12. X-ray diffraction patterns of Yb-0618 material prepared from β-Si_3N_4 powder at 1700°C for 50 h (highlighted) and 45 min Broader β' reflections in the latter case indicate that transient β'-SiAlON has a range of compositions.

reflections, and that after longer annealing these peaks sharpen toward lower 2θ values. This indicates that the initial β'-SiAlON contains less Al and O than the equilibrium β'-SiAlON. Note also that the structurally unrelated α'-SiAlON shows very little difference in its diffraction peaks after short-term and long-term annealing. Unlike reactions (1) and (2), though, there is not a significant variation in the amount of β'-SiAlON formed as the annealing time increases.

4 Discussion

4.1 The kinetic sequence of phase transformations

Our results described in Section 3 indicate a clear trend, i.e. the kinetics of phase transformations in Si_3N_4 and SiAlON ceramics follow the order (1) > (2) > (3) > (4). This order was established through direct comparisons involving various compositions; good systematics were achieved in all cases. In view of the shorter time and lower temperature used in our experiments, our results mostly pertain to the earlier stages of phase transformation (i.e. prior to coarsening). Indeed, the coarsening stage has been mostly avoided. To illustrate this point, Fig. 13 shows the SEM micrographs of Yb-0618 material prepared from α-Si_3N_4 powder and annealed at 1700°C for 45 min and 10 h. (The former time is representative of the time used in our work.) According to Fig. 3(a), the reaction is essentially complete after 45 min at 1700°C, and it yields a two-phase α'/β'-SiAlON mixture. However, the two phases cannot be easily differentiated by viewing Fig. 13(a), since the average grain size after 45 min annealing is still rather fine. Only after 10 h annealing [Fig. 13(b)], does the microstructure resemble those commonly seen for β-Si_3N_4. This indicates that the microstructure has not coarsened after 45 min even though the reaction is complete. Therefore, the order of the kinetics of phase transformations, (1) > (2) > (3) > (4) is already established before coarsening takes place.

4.2 Nucleation and growth

Since transformations (1)–(4) occur by precipitation from liquid, we can refer to the standard theory of nucleation and growth of crystallites from melt to draw some useful insight. According to this theory, the activation energy for formation of critical nuclei of a thermodynamically stable phase is given by the following expression:

$$\Delta E_a = \frac{16\pi\gamma^3 F(\theta)}{3(\Delta G)^2} \quad (1)$$

where γ is the liquid/solid interfacial free energy of the crystal, $F(\theta)$ is a geometrical factor (less than 1) that indicates the potency of heterogeneous nucleation, and ΔG is the driving force for transformation.

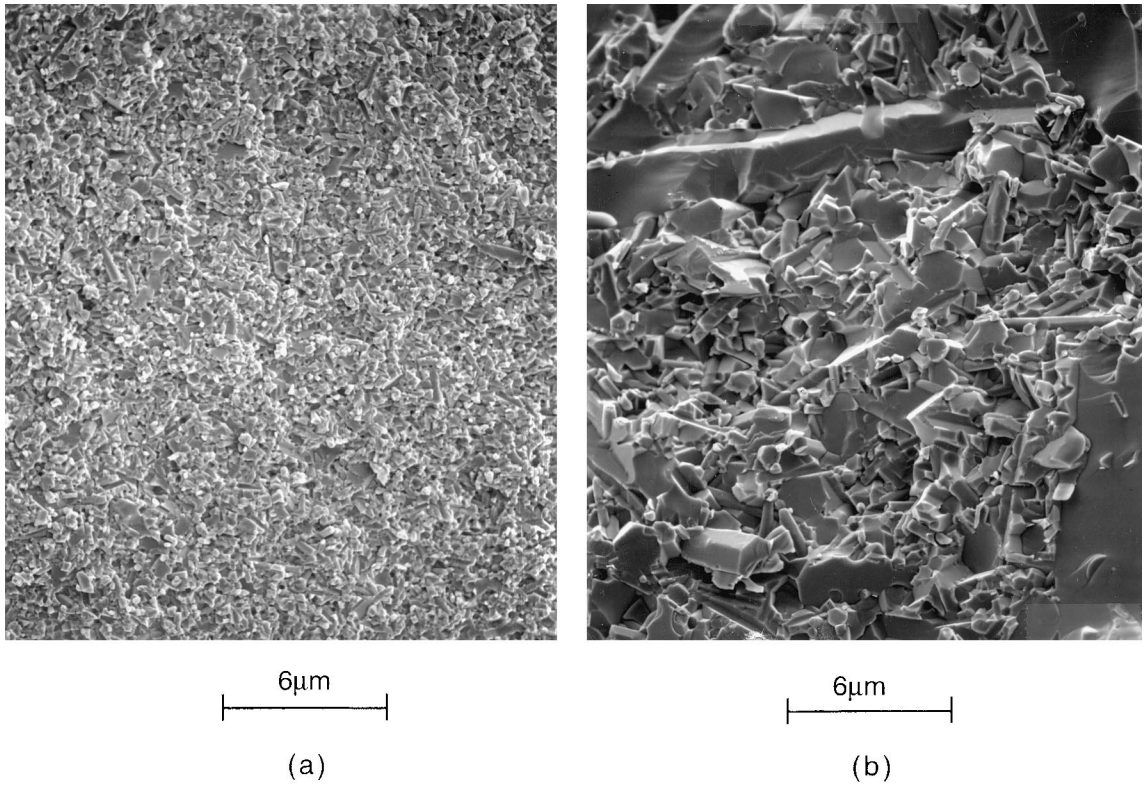

Fig. 13. SEM micrographs of fractured surfaces of Yb-0618 material prepared from α-powder at (a) 1700°C for 45 min and (b) 1700°C for 10 h. Much finer grain size is obtained in (a).

Nucleation rates are directly proportional to the activation energies by the following expression:

$$N = N_0 f_0 \exp\left(-\frac{\Delta E_a}{kT}\right) \qquad (2)$$

where f_o is a rate constant and N_o is the number of atoms in contact with the heterogeneous nucleation sites.

According to Eq. (1), activation energy is strongly affected by heterogeneous nucleation, via $F(\theta)$, and by driving force ΔG. A structural similarity between a nucleus and the product crystal decreases $F(\theta)$, enhancing the nucleation potency. A larger driving force lowers the activation energy regardless of the values of $F(\theta)$, i.e. the potency of nucleation. Both increase the nucleation rate and lead to faster overall kinetics. In addition, a larger number of structurally related nucleation sites increases N_0 in eqn (2), which also leads to faster overall kinetics. Of the above three factors, a larger ΔG is probably the most important since it lowers the activation energy given in eqn (1) in a very strong way, and the activation energy enters eqn (2) exponentially with a very large effect on the overall kinetics.

With the above knowledge and with the assumption that heterogeneous nucleation sites, isostructural with the product phase, are available, it is now easy to understand the kinetic sequence (1) > (2) > (3) > (4). Reaction (1) is faster than (2), when α' and β' are in equilibrium, because of a larger number of atoms in contact with heterogenous nucleation sites (i.e. N_o) in reaction (1). This also applies to reaction (3) and (4), with (3) > (4). Comparing reaction (2) and (3), we see that although reaction (3) may enjoy some advantage in N_o, the larger driving force in reaction (2) may lower the nucleation barrier ΔE_a sufficiently for heterogeneous nucleation to yield a faster nucleation rate. Lastly, the comparison of reactions (1) and (4) is trivial, since N_o, ΔE_a and ΔG all favor reaction (1) in this case. Therefore, the reaction sequence (1) > (2) > (3) > (4) can be completely rationalized by the schematic energetic considerations shown in Fig. 1 after taking into account the number of isostructural heterogeneous nucleation sites in each case.

Although the above interpretation relies entirely on the efficacy of heterogeneous nucleation, by recognizing that structurally similar seed powders always exist in our experiments, the nucleation argument can still apply even if homogeneous nucleation has to intervene in reactions (2) and (4). In the latter scenario, reaction (1) is clearly favored over reaction (4), because heterogeneous nucleation [$F(\theta)$ is small] is more potent than homogeneous

nucleation [$F(\theta)$ is close to unity]. On the other hand, the observation that reaction (2) is faster than reaction (3) suggests that, in reaction (2), a larger ΔG can decrease ΔE_a sufficiently to offset the adverse effect of a larger $F(\theta)$. Thus, the kinetic sequence (1) > (2) > (3) > (4) still holds even in this scenario if we allow a sufficiently large effect of ΔG on ΔE_a.

In the above discussion, we have not considered the role of growth in phase transformation. The growth rate is expected to increase monotonically with the driving force and thus its effect on the transformation kinetics cannot be easily separated from that of nucleation. Moreover, in the case of α'-SiAlON, our study in Paper I has shown that the stability of α'-SiAlON increases with temperature; therefore, a larger driving force is expected at higher temperatures for reactions (1) and (4). This is unlike the case of crystallization from melt, in which the driving force decreases with temperature. Therefore, it is not possible to take advantage of the two distinct temperature regions, controlled by nucleation and growth (as in the case of crystallization from melt) to separate the roles of nucleation and growth in transformations described here. The growth argument alone would suggest that reactions (1) and (2) are faster than reactions (3) and (4), but it could not distinguish between reactions (1) and (2), nor between reactions (3) and (4). On the other hand, there is evidence from this study that seems to suggest that nucleation is probably the more important, if not the controlling factor. For example, the difference in T_{50} in Fig. 6 between reactions (3) and (4) are much larger than those in Fig. 3 between reactions (1) and (2). Since the reactions in each pair occur under the same driving force, the difference in the growth rate should be small and should not lead to a large spread in T_{50} anyway. From the viewpoint of nucleation, however, these difference can be readily explained in terms of differences in N_0. Furthermore, it is known that with a decreasing ΔG, the potency of nuclei becomes all the more important. So the difference between structurally similar and structurally dissimilar starting powders in relation to the product phase also becomes greater. This explains why ΔT_{50} is larger in reactions (3) and (4) than in reaction (1) and (2). The same effect is again seen in comparing reactions (1) and (4). As we previously noted in Section 3.4 the decrease of ΔG (for forming α'-SiAlON) from Yb-1212 to Yb-1020 causes a large shift of 200°C in T_{50} in reaction (4), which has a smaller ΔG overall. This compares with very little shift in reaction (1) which has a large ΔG overall. Presumably, this is also caused by the highly non-linear dependence of the nucleation rate on the driving force.

4.3 Coherent nucleation

The observation of transient evolutions described in Section 3.6 offers yet another piece of evidence that the nucleation consideration is important and that isostructural nucleation is favored in SiAlON phase transformation. In comparing reactions (1) and (2), with α'-SiAlON in equilibrium with β'-SiAlON, the driving force is identical, so the formation of α'-SiAlON and β'-SiAlON should have proceeded in a similar way. The fact that a product phase of non-equilibrium composition forms only in the case of structurally related phases implies that this path is favorable despite the higher free energy of the non-equilibrium compositions. A similar situation is also seen in comparing reactions (3) and (4). The advantage of the non-equilibrium composition, which is lean in solute, is that it has a lattice parameter much closer to the structurally-related starting powder. For example, an α'-SiAlON lean in solute is closer in structure to α-Si_3N_4 than is an α'-SiAlON rich in solute. Likewise, a β'-SiAlON lean in solute is structurally closer to β-Si_3N_4 than is a β'-SiAlON rich in solute. This in turn means a smaller misfit at the interface and a lower interfacial energy and strain energy for the nucleus, leading to a smaller nucleation barrier ΔE_a. This modified ΔE_a (albeit at a lower ΔG because of non-equilibrium) is apparently smaller than the unmodified ΔE_a for the equilibrium composition. As a result, phase transformation to a product phase of non-equilibrium composition occurs. Presumably, the availability of a large number of structurally similar starting powder, as in reaction (1) and reaction (3), allow these non-equilibrium reactions to proceed more prominently and to be detected by XRD more easily.

Transformation of the above type, which assumes non-equilibrium composition in order to maintain nucleation advantage, is called coherent transformation in the literature.[8] Here, coherency refers to the close match of the lattice structures of the product and the parent phases, as in the case of $\alpha \rightarrow \alpha'$-SiAlON and $\beta' \rightarrow \beta'$-SiAlON transformations. Phase diagrams under the constrained equilibrium condition of coherent transformation generally show a phase boundary that is shifted from the equilibrium phase boundary. Therefore, the phase amount of the coherent transformation determined by the lever rule applied to the coherent phase diagram could be different from the phase amount expected for equilibrium transformations.

In the case of SiAlON transformations, coherent transformation obviously favors a product SiAlON phase that is leaner in solute. (All solutes tend to expand the lattice Si_3N_4 in both α and β form.) Thus, it follows that the coherent α' (or β') phase boundary is leaner in solute composition than its

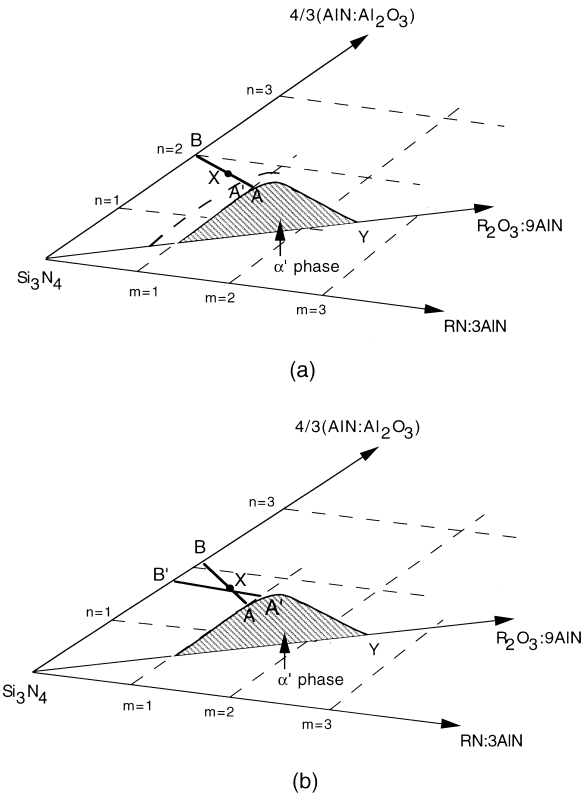

Fig. 14. (a) Schematic phase diagram showing equilibrium α'-boundary and coherent α'-boundary (dashed line). In the two-phase composition X the fraction of α' is higher for coherent α' precipitation ($XB/A'B > XB/AB$). (b) Coherent tie-line of β'-SiAlON ($B'A'$) and equilibrium tie-line of β'-SiAlON (BA). The phase fraction is similar in both cases for the same composition X since AA' is nearly parallel to BB'.

equilibrium counterpart. In comparing reactions (1) and (2), we used a composition that falls in the two-phase region. As the coherent α' phase boundary moves toward the Si_3N_4–AlN:Al_2O_3 line [see Fig. 14 (a)], simple application of the lever rule leads to the conclusion that the amount of the transient coherent α' should be more than the equilibrium incoherent α'. This is exactly what was observed in our experiments. In comparing reactions (3) and (4), of the same two-phase composition, on the other hand, the shift of the coherent β' phase boundary is along the Si_3N_4–AlN:Al_2O_3 line and is not toward the R_2O_3:9AlN direction [see Fig. 14 (b)]. Therefore, the relative positions of the β' line (Si_3N_4–AlN:Al_2O_3) and α' boundary are essentially the same and it does not create a significant difference in the amount of phase upon application of the lever rule (only the tie-line is changed). Indeed, as we mentioned earlier we failed to observe a significant change in the amount of β'-SiAlON in comparing reactions (3) and (4). Nevertheless, XRD evidence of non-equilibrium β'-SiAlON with a leaner Al and O composition was seen and this is consistent with the above analysis. Finally, as the transformation product grows in size during further annealing, coherency is broken to relieve the strain energy and after that the composition must be re-equilibrated to approach the equilibrium value. In so doing, both the amount and the composition of the product phase revert to the ones expected for the equilibrium phase diagrams. Presumably, this would involve some solution-reprecipitation of the non-equilibrium phase if solid state diffusion is too sluggish. Microscopic evidence of this aspect, however, has not been collected in the present work and must await future studies.

Interestingly, it has been reported in the literature that when α-Si_3N_4 is used as starting powder to form β'-SiAlON [reaction (2)], quite often the first β' grains are richer in Al and O than the overall composition,[9,10] in contrast to our observation conducted with β-Si_3N_4 starting powder. Since the free energy of β'-SiAlON obviously decreases initially as the amount of Al–O increases, the above observation is consistent with the idea that ΔG is the controlling factor for nucleation. The Al–O-rich composition would then be possible if the early nucleation is homogeneous in nature so that the coherency strain is not an issue, or if ΔG for reaction (2) is initially so large that it overrides the strain energy consideration. On the other hand, the availability of a large number of β-Si_3N_4 sites and the lower driving force for reaction (3) can obviate these conditions. This could then explain why heterogeneous coherent nucleation is favored in our experiment.

5 Conclusions

- SiAlON formation using α-Si_3N_4 starting powders proceeds faster than using β-Si_3N_4 starting powders, because of a higher driving force for the less stable α powders.
- In two-phase reactions when both α' and β'-SiAlON form, the SiAlON phase that is structurally similar to the majority of the starting powders forms faster.
- Transient evolutions in the two-phase reactions indicate that coherent nucleation on isostructural sites occurs, giving an initial composition that is leaner in solute than the equilibrium composition.

Acknowledgements

Supported by the Air Force Office for Scientific Research, Grant No. F49620-98-1-0126. The use of facilities in the Laboratory for Research on the Structure of Matter at the University of Pennsylvania, supported by the National Science Foundation under MRSEC Grant No. DMR 96-32598, is also acknowledged.

References

1. Priest, H. F., Burns, F. C., Priest, G. L. and Skaar, E., Oxygen content of alpha silicon nitride. *J. Am. Ceram. Soc*., 1973, **56**(7), 395.
2. Grun, R., The crystal structure of β-Si_3N_4; structural and stability considerations between α- and β-Si_3N_4. *Acta Cryst. B*, 1979, **35**, 800–804.
3. Hwang, S.-L. and Chen, I.-W., Nucleation and growth of α'-SiAlON on α-Si_3N_4. *J. Am. Ceram. Soc*., 1994, **77**(7), 1711–1718.
4. Hwang, S.-L. and Chen, I.-W., Nucleation and growth of β'-SiAlON. *J. Am. Ceram. Soc*., 1994, **77**(7), 1719–1728.
5. Rosenflanz, A. and Chen, I. -W., Phase relationships and stability of α'-SiAlON, *J. Am. Ceram. Soc*., 1999, 82(4) 1025–1036.
6. Shen, Z. Nordberg, L. -O. Nygren, M. and Ekstrom, T., In *Proc. Nato AST Engineering Ceramics 96—Higher Reliability through Processing*, ed. G. N. Babini. Kluwer Academic, Dordrecht, 1997, pp. 169–178.
7. Kato, A., Sarugaku, K. and Sameshima, S., Sinterability of silicon nitride powders. In *High-Tech Ceramics*, ed. P. Vincenzini. Elsevier, Amsterdam, 1987, pp. 911–924.
8. Porter, D. A. and Easterling, K.E., *Phase transformations in metals and alloys*. Chapman and Hill (Printed in UK by T. J. Press Ltd., Padstow, Cornwall, 1981).
9. Bonnell, D. A. Determination of crystallization mechanisms and correlation of grain-boundary morphology to mechanical properties in silicon nitride, Ph.D thesis, University of Michigan, Ann Arbor, MI, 1986.
10. Hwang, S.-L. and Chen, I.-W., Reaction hot pressing of $\alpha'-$ and β'-SiAlON ceramics. *J. Am. Ceram. Soc*., 1994, **77**(1), 165–171.